Applied Physics Letters

Acoustic multi-layer Helmholtz resonance metamaterials with multiple adjustable absorption peaks

Cite as: Appl. Phys. Lett. **118**, 241904 (2021); https://doi.org/10.1063/5.0054562
Submitted: 19 April 2021 • Accepted: 01 June 2021 • Published Online: 17 June 2021

Haiqin Duan, Xinmin Shen, Enshuai Wang, et al.

Applied Physics Letters ARTICLE scitation.org/journal/apl

Acoustic multi-layer Helmholtz resonance metamaterials with multiple adjustable absorption peaks

Cite as: Appl. Phys. Lett. **118**, 241904 (2021); doi: 10.1063/5.0054562
Submitted: 19 April 2021 · Accepted: 1 June 2021 ·
Published Online: 17 June 2021

Haiqin Duan, Xinmin Shen,[a] Enshuai Wang, Fei Yang, Xiaonan Zhang, and Qin Yin

AFFILIATIONS

Department of Mechanical Engineering, Field Engineering College, Army Engineering University of PLA, No. 1 Haifu Street, Nanjing 210007, China

[a]Author to whom correspondence should be addressed: shenxmjfjlgdx2014@163.com. Tel.: +86-025-8082-1451

ABSTRACT

The single Helmholtz resonator obtains only one absorption peak in the broad frequency range, which limits its application in reducing the noise with multiple spectra. This paper reports an acoustic multi-layer Helmholtz resonance metamaterial, which can achieve multiple absorption peaks at given low-frequency targets. Meanwhile, through adjusting structural parameters of the multi-layer Helmholtz resonator, its impedance can be altered correspondingly to realize the absorption of noise with the multi groups of specific frequencies. In this paper, in order to achieve fine absorption performance with the specific frequencies of 100 and 400 Hz for a substation noise source, the sound absorption principle of a classical Helmholtz resonator with the embedded aperture is introduced theoretically, and then two series of multi-layer Helmholtz resonance structures with different parameters are designed. Thickness of the multi-layer structure is only 1/30th of the working wavelength, and two groups of resonance peaks are generated at 100 and 400 Hz, respectively. A finite element model of the multi-layer Helmholtz resonator is constructed to simulate its absorption performance. The samples are fabricated through the 3D light-curing printing, and their sound absorption performances are detected by the standing wave method. The simulation results are in good agreement with the experimental data, and two peaks with near-perfect absorptions are achieved at the target frequencies. The multi-layer Helmholtz resonator for achievement of three groups of absorption peaks is proposed later. This work provides an effective method to design a sound absorber with multiple absorption peaks, which can promote the application of acoustic metamaterials.

The noise pollution has serious impact on the people's healthy living, and a series of sound-absorbing materials are proposed for noise control.[1] However, low-frequency sound absorption has been a challenging topic for the researchers due to the weak energy dissipation in traditional materials.[2] To absorb the low-frequency sound waves, a very thick structure (for porous material)[3] or a very long rear cavity (for microperforated panel)[4] is required inevitably. In recent years, the subwavelength acoustic metamaterials (AMs) with the excellent low-frequency sound absorption performance have provided an effective way to solve the problem of low-frequency noise such as membrane-type AMs[5–9] and cavity-based AMs.[10–13] Based on the classic Helmholtz resonator, its ability to be treated as a perfect sound absorber with a deep subwavelength thickness has been well established.[14–21]

The most effective way to realize broadband sound absorption is to introduce the multiple detuned units with the different absorption peaks.[22–28] For example, Zhang and Hu[25] reported a six-unit coiled-up structure to achieve perfect absorption performance. Peng *et al.*[26] demonstrated a composite honeycomb metasurface panel, which is comprised of arranged honeycomb "supercells" that consist of unit cells of different geometric parameters, and sound absorption coefficients of 0.9 in 600–1000 Hz were achieved. However, a detuned resonance unit can produce only one narrowband absorption peak. It is extremely challenging to broaden the sound absorption band under the constraints of the limited thickness and size. One effective strategy for generating additional absorption peaks is to use a multi-layer arrangement.[19,29,30] Liu *et al.*[29] reported a perforated composite Helmholtz-resonator that could obtain multiple near-perfect peaks in higher frequencies by inserting one or more separating plates with a small hole into the interior of a Helmholtz resonator. Guo *et al.*[30] had developed a structure consisted of the multi-layer Helmholtz

resonators (MHRs) with extended necks, which induced the additional absorption peaks. These research provide promising references to absorb the noises with various peaks. However, the cavity diameter of the multi-layer arrangement is consistent with that of the upper layer, which makes it difficult to obtain multi-order absorption peaks by adjusting the parameters.

In this work, based on the principle of local resonance of the Helmholtz resonator, we propose a type of acoustic metamaterial as the multi-layer Helmholtz resonator (MHR), in which the number of the resonance unit increases layer by layer. The sound wave enters MHR from the air medium and causes the resonance of structural unit in the MHR. The local resonance greatly enhances the sound energy density and results in the energy dissipation to gain the perfect sound absorption.[31] In the low-frequency range, the combining effect of two Helmholtz acoustic absorbers with different parameters can realize the approximate perfect sound absorption with two groups of specific frequencies, and the thickness is only 1/30th of the working wavelength. In addition, the Helmholtz resonators with embedded apertures are used as the basic unit to control the impedance of the multi-layer structure, and the sound absorption frequency of the structure is adjusted by selecting the diameter and length of the resonator under the condition of keeping its external dimension invariant.

To illustrate the combining effect of the MHR, we first analyze the Helmholtz acoustic system. If the linearity of an acoustic element is much smaller than the wavelength of the sound, the propagation of sound can be temporarily ignored, and the movement of all parts of acoustic element can be considered as uniform. The structure of Helmholtz resonator is shown in Fig. 1(a), where D is the diameter of the cavity, S is the cross-sectional area of the short tube (the diameter is d), and l is the length of the short tube. Assuming that the structure meets the following conditions:

(1) The linearity of the Helmholtz resonator is much smaller than the wavelength of the sound wave, which is d, l, $\sqrt[3]{V_0} \ll \lambda$.
(2) The volume of the short tube is much smaller than the volume of the cavity, which is $Sl \ll V_0$.
(3) The cavity wall is a hard boundary, which will not deform under the action of sound pressure.

According to assumption (1), the linearity of the short tube is much smaller than the wavelength, so the vibration in the short tube can be considered as uniform, and the air column in the short tube can be treated as a whole with a mass of $M_m = \rho_0 l_0 S$. Taking into account the radiation of the sound waves, length of the short tube is revised as $l = l_0 + 0.85d$. The frictional resistance between the vibration of the air column and the short tube wall is R_m.

The air in the cavity will be compressed or expanded with the movement of the air column in the short tube. The force of the cavity acting on the air column of the short tube is equivalent to the elastic force generated by a spring, and its elastic coefficient is $K_m = \frac{\rho_0 c_0^2 S^2}{V_0}$. Meanwhile, the corresponding reciprocal denotes the compliance $C_m = \frac{1}{K_m} = \frac{V_0}{\rho_0 c_0^2 S^2}$.

According to the above analysis, it can be concluded that the Helmholtz resonator contains three components: mass, force resistance, and compliance. When the entrance of the tube is subjected to sound pressure $p = p_a e^{j\omega t}$, the motion equation of air column of the short pipe is as follows:

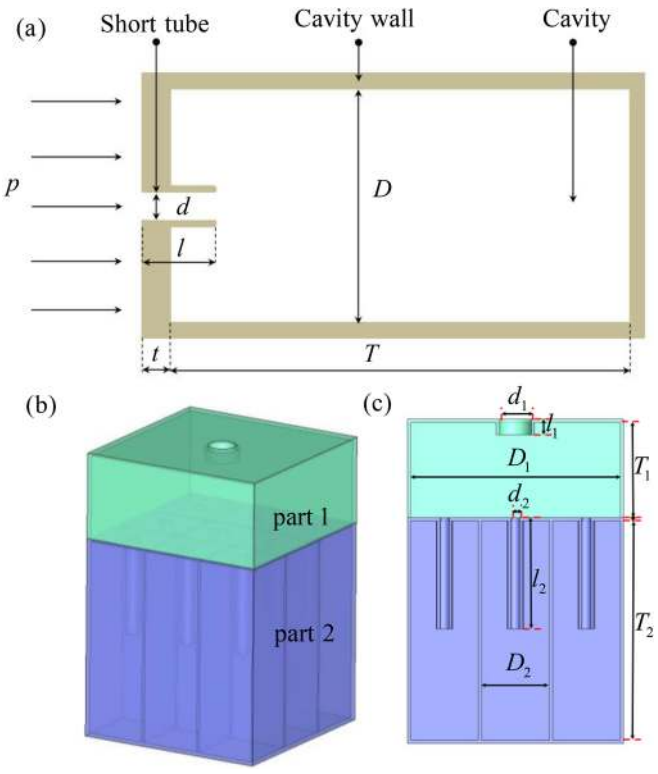

FIG. 1. The Helmholtz acoustic system. (a) Schematic diagram of the Helmholtz resonator with the embedded apertures. (b) Three-dimensional structural model of MHR. (c) Half-sectional view of MHR, here, d and l represent diameter and length of apertures, respectively; D and T are the diameter and length of the cavity, respectively.

$$M_m \frac{d^2\xi}{dt^2} = Sp_a e^{j\omega t} - R_m \frac{d\xi}{dt} - \frac{1}{C_m}\xi. \tag{1}$$

Here, they can be symboled as $M_a = \frac{M_m}{S^2}$, $R_a = \frac{R_m}{S^2}$, and $C_a = C_m S^2$, in which M_a, R_a, and C_a represent the sound quality, sound resistance, and sound capacity (or sound compliance), respectively. By this method, Eq. (1) can be further converted as the following equation:

$$M_a \frac{dU}{dt} + R_a U + \frac{1}{C_a}\int U dt = p_a e^{j\omega t}. \tag{2}$$

By solving Eq. (2), it gives

$$U = \frac{p}{Z_a}. \tag{3}$$

The acoustic impedance of the Helmholtz resonator is

$$Z_a = \frac{p}{U} = R_a + j\left(\omega M_a - \frac{1}{\omega C_a}\right). \tag{4}$$

The constructed theoretical model of MHR in this work can be treated as a preliminary feasibility analysis of its sound absorption characteristics. See the supplementary material for the theoretical model in detail.

The single Helmholtz resonator has only one set of absorption peak in the low-frequency range. However, the present study indicated that combining multiple Helmholtz resonance units together can produce multiple absorption peaks. The resonance frequency of the Helmholtz resonator is related to the diameter of the cavity, length of the cavity, and diameter and length of the short tube. In order to achieve the low-frequency noise reduction within a small size, the MHR with the embedded aperture is adopted, which reduces the occupied space. In addition, the impedance of the Helmholtz resonator can be easily controlled by adjusting length of the embedded aperture. Taking the Helmholtz resonator as a basic unit, the MHR structure shown in Fig. 1(b) is optimized by precisely adjusting the structural combination of two different parameters. The optimization parameters are obtained by the neural network algorithm, and the optimization model based on the neural network can greatly improve the optimization efficiency (see the supplementary material for details). The MHR structure consists of two parts. The first part is a single-layer Helmholtz resonator, and the second part is nine Helmholtz resonators with same structural parameters. The selected structural parameters are as follows: $T_1 = 29$ mm, $T_2 = 68$ mm, $D_1 = 65.76$ mm, $D_2 = 21.25$ mm, $d_1 = 10$ mm, $d_2 = 3$ mm, $l_1 = 10$ mm, $l_2 = 35$ mm, and $t = 1$ mm. The two parts are combined in series. Form and parameters of the structure are not fixed, and it can be optimized according to the required absorption frequency in the practical application.

In order to effectively reveal the combining effect of sound absorption in the MHR, a finite element simulation model is constructed, and the pressure-acoustic model of the acoustic module in the model is used to simulate the physical field. The main reason for the sound dissipation of the Helmholtz resonator is that the oscillation of the air inside the cavity will make most of the sound energy to dissipate at the holes when the resonance frequency is reached. Narrow acoustic boundary conditions are set at aperture of the cavity in the model to fully consider the thermal viscosity loss of the structure. The simulation model is shown in Fig. 2(a). The figure shows the internal air cavity of the structure. The contact surface between the structure wall and internal air is set as a rigid wall. The type of background pressure field (BPF) is plane wave. The sound pressure is $|p_b| = 1$ Pa, and wave vector is $e_k = (0, 0, -1)$. The maximum mesh of embedded aperture is set as $d_i/5$, and the minimum mesh is $d_v/2$, where $d_v = \sqrt{2\mu/\rho_0\omega}$ is the thickness of the viscous boundary layer. A free tetrahedral mesh is used throughout the air cavity, and the maximum size is $D_i/10$. In order to accurately calculate the thermal viscosity loss of the boundary layer, six boundary layer meshes are applied on the hole and cavity wall, and the thickness of each layer is $d_v/4$. The perfect matching layer (PML) with eight layer meshes constructed by sweeping is established to absorb all outgoing waves, and frequency domain analysis is used to sweep the frequency analysis (see the supplementary material for details).

To verify the effectiveness of the simulation model, the experimental samples were made with resin materials through the 3D light-curing printing technology.[32] The 3D model of the sample is built by 3D modeling software, processed by slicing software, and imported into the 3D printer for manufacturing. The produced sample is shown in Fig. 2(b). AWA6128A standing wave tube tester is mainly used to

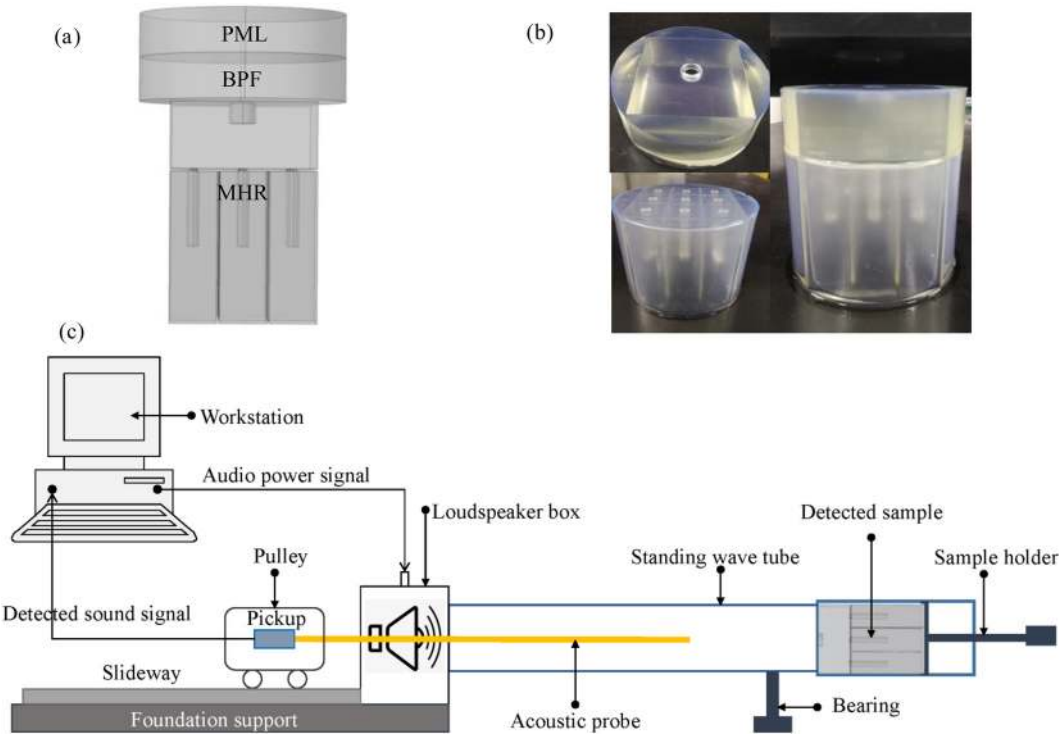

FIG. 2. Simulation and detection of the MHR. (a) The simulation model of MHR, in which the upper part of the cylinder is a perfectly matched layer and the lower part is a plane wave physical field. (b) 3D-printed experimental samples. (c) Schematic diagram of the AWA6128A standing wave tube tester.

measure the sound absorption coefficients of the materials,[33] as shown in Fig. 2(c). According to the sound levels of peak points and valley points measured by the test microphone in the standing wave tube, the instrument can automatically calculate the sound absorption coefficient by the solution software. The calculation formula of a sound absorption coefficient is as follows:[34]

$$\alpha = \frac{4 \times 10^{L/20}}{\left(1 + 10^{(L/2)}\right)^2}, \tag{5}$$

where L is the difference between the peak value and valley value of the sound pressure level.

The experimental and simulation results of the sound absorption coefficients in the frequency range of 50–600 Hz are summarized in Fig. 3. It can be observed that two near-perfect absorption peaks in simulation were obtained at 110 and 392 Hz, respectively, and those in the experiment were achieved at 105 and 405 Hz, respectively. The distribution of sound pressure can clearly exhibit the acoustic energy density inside the structure. According to the sound pressure level diagram of the two peak absorption frequencies [as shown in Figs. 3(a) and 3(b)], there are great differences in the distribution of acoustic energy density at resonance frequencies. Part 2 and part 1 of acoustic energy density driven by sound wave fluctuation have been found significantly increased near 110 and 392 Hz, respectively. It can be concluded that the first absorption peak is mainly caused by the dissipation of the MHR in part 2, and the second absorption peak is caused by the dissipation of the MHR in part 1.

Distribution of the sound absorption coefficient in simulation is in good agreement with that of the experimental result in Fig. 3, and the maximum error of the two groups of absorption peaks is within 5%, which proves the effectiveness of the simulation model. The failure to reach 100% absorption at the resonance frequency is due to the incomplete match between the impedance of the MHR and air, which can be further optimized through adjusting the parameters of MHR. The difference in peak absorption frequency between simulation and experimental results is mainly due to the dimension error caused by machining accuracy. It can be seen from the distribution of a sound pressure level that the sound energy dissipation of the first absorption peak is mainly caused by the strong resonance of the second part of the MHR, and the second absorption peak is caused by the first part of the MHR. Since the second part of the structure is composed of nine chambers, the machining error leads to the inconsistency of diameter and other parameters among the nine chambers, which is the main reason for that the first absorption peak of the experimental value is lower than the simulation data and the near-perfect sound absorption cannot be achieved. In addition, because the surface of the 3D printed sample is not absolutely smooth, the sound absorption coefficient in the experiment is significantly higher than that in the simulation at the corresponding frequency point for the acoustic scattering.

This design method is not just applicable to the prospect of two sets of peaks. We design the three groups of structural models with different parameters. Model 1 consists of a single Helmholtz resonator, model 2 consists of two sets of Helmholtz resonators with different parameters, and model 3 consists of three sets of Helmholtz resonators with different parameters, as shown in Fig. 4(b). Meanwhile, the specific parameters for these structural models are summarized in Table I.

The simulation results are shown in Fig. 4(a). It can be observed that the absorption peak can reach more than 95%. As the number of cavities increases, the embedded aperture gradually becomes shorter. At the same time, diameter of the aperture is positively related to the volume of the cavity. The additional peaks emerge as a result of combining the metamaterial with the waveguide when the number of cavities in series increases. It can be further found that the first absorption peaks of the three models and the second absorption peaks of model 2 and model 3 are closer, because acoustic impedance of the MHR is actually consisted of the acoustic capacitance of air cavity and the acoustic mass and acoustic resistance of the embedded neck. The

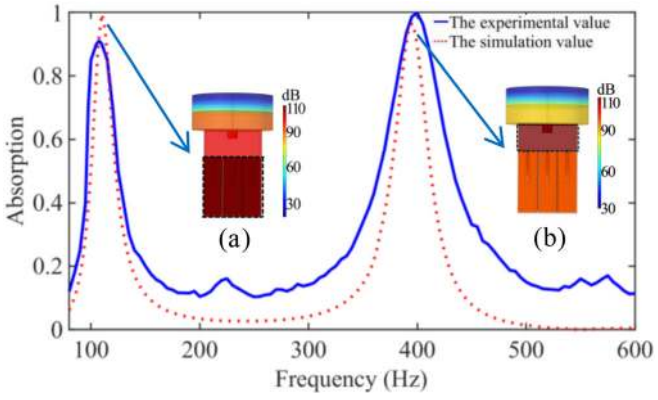

FIG. 3. The experimental and simulation results of sound absorption coefficients of the investigated MHR. (a) and (b) are the simulation sound pressure level diagrams of the perfect absorption peaks of MHR at 110 and 392 Hz, respectively.

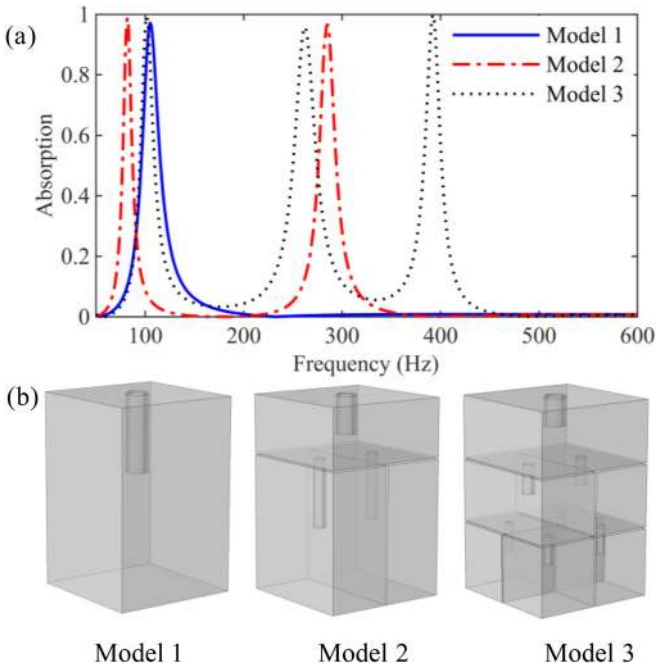

FIG. 4. Investigation of the MHR with variable layer. (a) Sound absorption simulation results of the three groups of MHR with variable layer. (b) 3D model drawing of model 1, model 2, and model 3.

TABLE I. Specific parameters of the structural model (mm).

Model	T_1	T_2	T_3	D_1	D_2	D_3	d_1	d_2	d_3	l_1	l_2	l_3
1	99	···	···	65.76 × 65.76	···	···	5	···	···	40	···	···
2	29	68	···	65.76 × 65.76	65.76 × 32.38	···	9	5	···	20	35	···
3	32	32	32	65.76 × 65.76	65.76 × 32.38	32.38 × 32.38	10	5	3	15	15	15

sound quality M_a is determined by the quality of the air column in the embedded aperture, and the sound capacity C_a represents the elastic effect of the air in the rigid cavity.

In summary, we have proposed and experimentally demonstrated an acoustic multi-layer Helmholtz resonance metamaterial to achieve the perfect sound absorption of low-frequency multi-group noise. By combining the local resonance of Helmholtz resonator with the different parameters, we design MHR structure that can generate multiple sets of absorption peaks and accurately control the peak absorption frequency. We verify our ideas through finite element simulations and conduct an experiment for further validation by testing the 3D printed sample. Both experimental and simulation results demonstrate that the MHR can achieve almost perfect sound absorption with sub-wavelength structure size. The proposed structure is an innovative extension of the classic Helmholtz resonator and has a promising application in the field of multi-frequency noise reduction.

See the supplementary material for the theoretical modeling, neural network optimization, and numerical analysis method in detail.

This work was supported by the Natural Science Foundation of Jiangsu Province (Grant Nos. BK20201336 and BK20150714) and the National Natural Science Foundation of China (Grant No. 51505498).

DATA AVAILABILITY

The processed data that support the findings of this study are available within the article and its supplementary material. The processed data that support the findings of this study are available from the corresponding author upon reasonable request.

REFERENCES

[1]P. Sheng, J. Acoust. Soc. Am. **141**, 3575 (2017).
[2]M. Y. Duan, C. L. Yu, Z. M. Xu, F. X. Xin, and T. J. Lu, Appl. Phys. Lett. **117**, 151904 (2020).
[3]Y. Li and B. M. Assouar, Appl. Phys. Lett. **108**, 063502 (2016).
[4]D. Y. Maa, J. Acoust. Soc. Am. **104**, 2861 (1998).
[5]J. J. Zhao, X. H. Li, Y. Y. Wang, W. J. Wang, B. Zhang, and X. L. Gai, J. Acoust. Soc. Am. **141**, 840 (2017).
[6]S. H. Lee, C. M. Park, Y. M. Seo, Z. G. Wang, and C. K. Kim, Phys. Rev. Lett. **104**, 054301 (2010).
[7]N. Jiménez, W. Huang, V. Romero-García, V. Pagneux, and J.-P. Groby, Appl. Phys. Lett. **109**, 121902 (2016).
[8]Z. Yang, H. M. Dai, N. H. Chan, G. C. Ma, and P. Sheng, Appl. Phys. Lett. **96**, 041906 (2010).
[9]G. C. Ma, M. Yang, S. W. Xiao, Z. Y. Yang, and P. Sheng, Nat. Mater. **13**, 873 (2014).
[10]H. Q. Min and W. C. Guo, Appl. Acoust. **149**, 123 (2019).
[11]X. Y. Peng, J. Ji, and Y. Jing, J. Acoust. Soc. Am. **144**, EL255 (2018).
[12]S. B. Huang, X. S. Fang, X. Wang, B. Assouar, Q. Cheng, and Y. Li, J. Acoust. Soc. Am. **145**, 254 (2019).
[13]L. J. Li, B. Zheng, L. M. Zhong, J. Yang, B. Liang, and J. C. Cheng, Appl. Phys. Lett. **113**, 103501 (2018).
[14]N. Fang, D. J. Xi, J. Y. Xu, M. Ambati, W. Srituravanich, C. Sun, and X. Zhang, Nat. Mater. **5**, 452 (2006).
[15]A. Merkel, G. Theocharis, O. Richoux, V. Romero-Garcia, and V. Pagneux, Appl. Phys. Lett. **107**, 244102 (2015).
[16]N. Jiménez, V. Romero-García, V. Pagneux, and J. P. Groby, Phys. Rev. **95**, 014205 (2017).
[17]X. X. Wu, C. X. Fu, X. Li, Y. Meng, Y. B. Gao, J. X. Tian, L. Wang, Y. Z. Huang, Z. Y. Yang, and W. J. Wen, Appl. Phys. Lett. **109**, 043501 (2016).
[18]V. Achilleos, O. Richoux, and G. Theocharis, J. Acoust. Soc. Am. **140**, EL94 (2016).
[19]Y. F. Tang, S. W. Ren, H. Meng, F. X. Xin, L. X. Huang, T. N. Chen, C. Z. Zhang, and T. J. Lu, Sci. Rep. **7**, 43340 (2017).
[20]T. A. Starkey, J. D. Smith, A. P. Hibbins, J. R. Sambles, and H. J. Rance, Appl. Phys. Lett. **110**, 041902 (2017).
[21]J. W. Guo, Y. Fang, Z. Y. Jiang, and X. Zhang, J. Phys. D **53**, 505504 (2020).
[22]C. R. Liu, J. H. Wu, F. Y. Ma, X. Chen, and Z. R. Yang, Appl. Phys. Express **12**, 084002 (2019).
[23]X. Jiang, B. Liang, R. Q. Li, X. Y. Zou, L. L. Yin, and J. C. Cheng, Appl. Phys. Express **105**, 243505 (2014).
[24]J. F. Li, W. Q. Wang, Y. B. Xie, B.-I. Popa, and S. A. Cummer, Appl. Phys. Lett. **109**, 091908 (2016).
[25]C. Zhang and X. H. Hu, Phys. Rev. Appl. **6**, 064025 (2016).
[26]X. Peng, J. Ji, and Y. Jing, J. Acoust. Soc. Am. **144**, EL255 (2018).
[27]R. A. Jahdali and Y. Wu, Appl. Phys. Lett. **108**, 031902 (2016).
[28]R. A. Jahdali and Y. Wu, Sci. Rep. **8**, 13855 (2018).
[29]C. R. Liu, J. H. Wu, X. Chen, and F. Ma, Appl. Phys. **52**, 105302 (2019).
[30]J. W. Guo, X. Zhang, Y. Fang, and Z. Y. Jiang, Compos. Struct. **260**, 113538 (2021).
[31]X. Zhang, Z. Qu, and H. Wang, iScience **23**, 101110 (2020).
[32]T. D. Ngo, A. Kashani, G. Imbalzano, K. T. Q. Nguyen, and D. Hui, Composites, Part B **143**, 172 (2018).
[33]H. Q. Duan, X. M. Shen, Q. Yin, F. Yang, and M. Pan, Appl. Acoust. **166**, 107322 (2020).
[34]X. C. Yang, K. Peng, X. M. Shen, X. N. Zhang, P. F. Bai, and P. J. Xu, Mater. Des. **131**, 297 (2017).